NORMAL STRESS DISTRIBUTION IN INFINITE ELASTIC MATRIX WITH A LOCALLY CURVED TRIPLE-WALLED CARBON NANOTUBE

by

Fatma Coban KAYIKCI[a] and Resat KOSKER[b*]

[a] Davutpasa Campus, Faculty of Chemistry and Metallurgy,
Yildiz Technical University, Esenler, Istanbul, Turkey
[b] Davutpasa Campus, Department Mathematical, Engineering, Faculty of Chemistry and Metallurgy,
Yildiz Technical University, Esenler, Istanbul, Turkey

Original scientific paper
https://doi.org/10.2298/TSCI200526009K

Nanocomposite materials are produced by using of nanotubes, the most significant structural elements of nanomaterials used in nanotechnologic applications. In the reinforcement (in the fibers) of the structure of composite materials, the appearance of the self-balancing stresses results from the initial curvature, caused by either structural reasons or technological processes. Because of exceeding safety limits of material caused by high magnitude self-balancing stresses, investigating the mechanical behaviors of the material theoretically, both under tensile and compression in the direction of strengthening (fiber) is essential for the engineering. Unlike the literature, in this study, composite materials containing triple-walled nanotube are investigated in the scope of the piecewise homogeneous body model by using of geometric non-linear exact equations of the 3-D theory of elasticity. The normal stress analysis, on the outermost surface of the carbon nanotube and the matrix intersection, is investigated under various external effects. Nanotube is first formed as having a small local curvature. Van der Waals forces existing between the carbon nanotube walls are taken into consideration.

Key words: *carbon nanotubes, triple-walled carbon nanotubes, stress analysis, geometric non-linearity, local curvature*

Introduction

Lately, the production of composite materials, which have superior properties than many other engineering materials, have started to rise significantly. They are rigid and light due to their high resistance and durability. Because of these features, establishing a mathematical model of their elastic behavior and investigating theoretically when they are exposed to various external forces is necessary. Among all type of composite materials, unidirectional fibrous composite materials play an important role. Periodic curvature and local curvature are the two categories of the primitive curvature status in composite materials. Periodic curvatures occur during design, whereas local curvatures occur as a result of technological processes. The success of composite materials in application after production depends upon both the determination of the stress-strain relations in the material and inclusion of this curvature in the calculations. As can be seen from sources Akbarov and Guz [1-5], Akbarov and Kosker [6, 7] aforementioned cur-

* Corresponding author, e-mail: kosker@yildiz.edu.tr

vatures cause the emergence of self-balancing stresses, which can reach enormous values and exceed the the resistance limit of composite due to the curvature and other related mechanical parameters. Therefore, establishing mathematical models of appropriate physical problems and investigating them theoretically is crucial, both in theory and in the application of composites. In [8], the situation of low density infinite length and single walled CNT embedded in polymer matrix is discussed and the stress distribution is examined depending on various parameters. Also, the study has been done in the scope of 3-D theory of elasticity within the framework of piecewise homogeneous body model.

Various studies are conducted on composites which contain CNT, the strongest-known materials nowadays. As can be seen from the examples of [9-11], there are many experimental and theoretical studies such as [12-18]. In recent years, many studies have focused on the mechanical behavior of single-walled and multi-walled CNT such as Ru [19], Shen [20], and Thai [21]. In particular, researches on single-wall and multi-walled CNT embedded in polymer and metal matrix materials are remarkable, [22, 23]. Applicability of continuous mechanics views in explaining the behavior of nanoobjects has been discussed in Young *et al.* [24], Guz [25], Duan *et al.* [26], and Windle [27]. Studies on the mechanical behavior of CNT and other types of nanostructures in areas where continuity approaches are applicable are discussed in Harik [28], Guz and Rushchidsky [29, 30].

As mentioned previously, the importance of nanocomposite materials (particularly nanotubes) has been increasing dramatically and the researches is being done about their mechanical behavior. In this study, unlike the studies in existing literature, the triple-walled carbon nanotube (TWCNT) with low density infinite length local curvature in the infinite environment (embedded in the matrix materials) has been taken into account and stress distribution has been investigated under various external effects. It can be seen from the literature summary that there is no study that develops an approximate analytical method for stress analysis in composite materials containing infinite length and locally curved TWCNT in the scope of 3-D elasticity. Therefore, this study, the stress distribution analysis on the intersectional surface of the outermost wall of the CNT and the matrix material surrounding it, is unique within the framework of the piecewise homogeneous body model with the use of the 3-D geometrically non-linear exact equations of the theory of elasticity as in [31]. Van der waals forces are also considered, which occurs between the layers as the number of walls in the nanotube increases [13].

Problem formulation

Single locally curved TWCNT embedded in the infinite length low density infinite elastic body is taken into account. Low density means that inter-TWCNT interaction is neglected. As in fig. 1, the locally curved TWCNT is modeled by concentric nesting of two hollow locally curved cylinders and it is assumed that there exists space between the cylinders [32]. In aforementioned model, it is thought that there are normal forces with intensity p that evenly distributed in the longitudinal direction of the CNT. Additionally, it is thought that the difference between the radial displacements of the adjacent surfaces of the tubes resists with van der Waals forces [12].

The cylindrical $Or\theta z$ and Cartesian $Ox_1x_2x_3$ system of co-ordinates is associated with the centerline of the nested nanotubes (TWCNT) as shown in fig. 1. Cylindrical and Cartesian co-ordinate systems are selected, and considered as Lagrange co-ordinates. It is thought that the evenly distributed normal forces with a density, ρ, in the direction of the nanotube, in the direction of Ox_3 (Oz), affect the infinite elastic body modeled previously and also the circular sections of radii of $R_1 = R - h^{(1)} - h^{(2)} - h^{(3)} - 2d$, $R_2 = R - h^{(1)} - h^{(2)} - 2d$, $R_3 = R - h^{(1)} - h^{(2)} - d$,

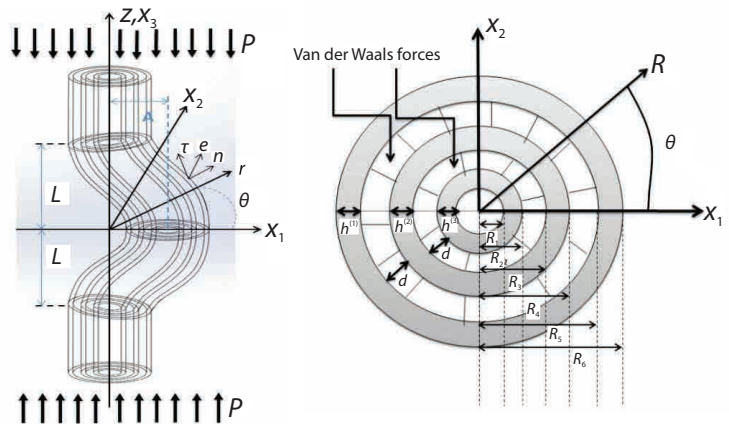

Figure 1. Geometry and co-ordinate systems of an infinitely elastic body containing TWCNT

$R_4 = R - h^{(1)} - d$, $R_5 = R - h^{(1)}$, and $R_6 = R$ perpendicular to the centerline of the nanotubes stay constant along the CNT. The radii R_1, R_2, R_3, R_4, R_5, and R_6 are also assumed to remain constant. The TWCNT and matrix materials are thought to be different from each other and linear elastic. Investigations have been made by using geometrically non-linear 3-D exact equations of continuum mechanics. Considering the geometry of the elastic body in fig. 1, the equation of the centerline of the nested nanotubes taken into account:

$$x_1 = F(x_3) = \varepsilon\delta(x_3), \quad x_2 = 0 \tag{1}$$

where ε ($0 \le \varepsilon < 1$) is a small parameter that specifies the bending amplitude of the CNT. On the other hand, the $\delta(x_3)$ function, shows the form of the bending of the CNT before loading. As seen from eq. (1), the middle line of the TWCNT with initial local curvature is on the $x_2 = 0$ plane. It is thought that the centerline of the CNT stays on this plane after loading. Using the equation of the middle line of the nanotube given with eq. (1) and the condition provided by the nanotube cross-section, the equation of the nanotube and matrix interface S_6 (the outermost surface of the outer tube), as shown in [3], can be obtained:

$$r(\ ,t\ ) = \frac{\varepsilon\delta(t_3)\left\{1+\varepsilon\ \left[\delta'(t_3)\right]\right\}\cos\theta}{1+\left[\delta'(\ \ )\right]\ \varepsilon^2\cos^2\theta} + \\ + \left(\frac{\varepsilon^2\left[\delta(t_3)\right]^2\left\{1+\varepsilon^2\left[\delta'(t_3)\right]^2\right\}\ \cos\theta}{\left\{1+\left[\delta'(\ \ )\right]\ \varepsilon^2\cos^2\theta\right\}} + R^2 \quad \left[\delta(t_3)\right]^2\varepsilon^2\left\{1+\varepsilon^2\left[\delta'(t_3)\right]^2\right\} \right)^{1/2} \tag{2}$$

$$x_3(\theta,t_3) = t_3 - \varepsilon\delta'(t_3)\left[r(\theta,\mathrm{t}_3) - \varepsilon\delta(t_3)\right],\ \ \delta'(t_3) = \frac{\mathrm{d}\delta(t_3)}{\mathrm{d}t_3}$$

where t_3 is the parameter and $t_3 \in (-\infty, +\infty)$. Through the eq. (2), the following equations are obtained for the components of the unit outer normal vectors of the S_6 surface [3]:

$$n_r = r(\theta,t_3)\frac{\partial z(\theta,t_3)}{\partial t_3}[A(\theta,z)]^{-1}$$
$$n_\theta = \left[\frac{\partial z(\theta,t_3)}{\partial \theta}\frac{\partial r(\theta,t_3)}{\partial t_3} - \frac{\partial r(\theta,t_3)}{\partial \theta}\frac{\partial z(\theta,t_3)}{\partial t_3}\right][A(\theta,z)]^{-1},\ n_z = -r(\theta,t_3)\frac{\partial r(\theta,t_3)}{\partial t_3}[A(\theta,t_3)]^{-1} \tag{3}$$

where $A(\theta, t_3)$

$$A(\theta,t_3) = \left\{\left[r(\theta,t_3)\frac{\partial z(\theta,t_3)}{\partial t_3}\right]^2 + \left[\frac{\partial z(\theta,t_3)}{\partial \theta}\frac{\partial r(\theta,t_3)}{\partial t_3} - \frac{\partial z(\theta,t_3)}{\partial t_3}\frac{\partial r(\theta,t_3)}{\partial \theta}\right]^2 + \left[r(\theta,t_3)\frac{\partial z(\theta,t_3)}{\partial t_3}\right]^2\right\}^{1/2} \tag{4}$$

After this, we will use the subscripts (1), (2), (3), and (4) to denote the quantities related to the matrix materials, the outer layer of TWCNT, middle layer of TWCNT and inner layer of TWCNT, respectively. Provided that it is satisfied in each of the layers of the TWCNT and the matrix material; it will be assumed that governing field equations will be provided:

$$\nabla_i\left[\sigma^{(l)ip}\left(g_p^j + \nabla_p u^{(l)j}\right)\right] = 0, \quad l = 1,2 \tag{5}$$

$$2\varepsilon_{jq}^{(l)} = \nabla_j u_q^{(l)} + \nabla_q u_j^{(l)} + \nabla_j u^{(l)n}\nabla_q u_p^{(l)} \tag{6}$$

$$\sigma_{(ip)}^{(l)} = \left[\lambda^{(l)}e^{(l)}\right]\delta_i^p + 2\left[\mu^{(l)}\varepsilon_{(ip)}^{(l)}\right],\ e^{(l)} = \varepsilon_{ii}^{(l)},\ i = 1,2,3 \tag{7}$$

In the eq. (7), $\sigma_{(ip)}^{(l)}$ and $\varepsilon_{(ip)}^{(l)}$ show the physical components of stress and strain tensors, respectively. At the same time, it will be assumed that the ideal contact conditions are satisfied on the nanotube and matrix interface S_6. These conditions are given as the outer normal vector components n_j of surface S_6:

$$\sigma^{(1)ip}\left[g_p^j + \nabla_p u^{(1)j}\right]\Big|_{S_6} n_j = {}^{(2)\mathrm{ip}}\left[g_p^j + \nabla_p u^{(2)j}\right]\Big|_{S_6} n_j,\ u^{(1)j}\Big|_{S_6} = u^{(2)j}\Big|_{S_6} \tag{8}$$

The boundary conditions between the outer surface of the middle tube, S_4, and the inner surface of the outer tube, S_5, can be written as the outer normal vectors of surfaces $n_j^{(l)}$ ($l = 2, 3$):

$$(R_5)\sigma^{(2)pp}\left(g_p^j + \nabla_p u^{(2)j}\right)\Big|_{S_3} n_j^{(\mathrm{l})} = c(u_p^{(2)}\Big|_{S_5} - u_p^{(3)}\Big|_{S_4}),\ \sigma^{(2)ip}\left(g_p^j + \nabla_p u^{(2)j}\right)\Big|_{S_5} n_j^{(\mathrm{l})} = 0,\ i = \tau, e$$
$$(R_5)\sigma^{(2)pp}\left(g_p^j + \nabla_p u^{(2)j}\right)\Big|_{S_5} n_j^{(\mathrm{l})} = (R_4)\sigma^{(3)pp}\left(g_p^j + \nabla_p u^{(3)j}\right)\Big|_{S_4} n_j^{(\mathrm{l})} \tag{9}$$
$$\sigma^{(3)ip}\left(g_p^j + \nabla_p u^{(3)\mathrm{j}}\right)\Big|_{S_4} n_j^{(\mathrm{l})} = 0,\ i = \tau, e$$

The boundary conditions between the outer surface of the inner tube, S_2, and the inner surface of the middle tube, S_3, can be written as the outer normal vectors of surfaces $n_j^{(l)}$ ($l = 2, 3$):

$$(R_3)\sigma^{(3)pp}\left(g_p^j + \nabla_p u^{(3)j}\right)\Big|_{S_3} n_j^{(\mathrm{l})} = c\left(u_p^{(3)}\Big|_{S_3} - u_p^{(4)}\Big|_{S_2}\right),\ \sigma^{(3)ip}\left(g_p^j + \nabla_p u^{(3)j}\right)\Big|_{S_3} n_j^{(\mathrm{l})} = 0,\ i = \tau, e$$
$$(R_3)\sigma^{(3)pp}\left(g_p^j + \nabla_p u^{(3)j}\right)\Big|_{S_3} n_j^{(\mathrm{l})} = (R_2)\sigma^{(4)pp}\left(g_p^j + \nabla_p u^{(4)j}\right)\Big|_{S_2} n_j^{(\mathrm{l})} \tag{10}$$
$$\sigma^{(4)ip}\left(g_p^j + \nabla_p u^{(3)j}\right)\Big|_{S_2} n_j^{(\mathrm{l})} = 0,\ i = \tau, e$$

The following condition is satisfied on the inner surface, S_1, of the inner tube with radius R_1, fig. 1. The outer normal vector components are $n_j^{(1)}$:

$$\sigma^{(4)ip}\left[g_p^j+\nabla_p u^{(4)j}\right]\Big|_{S_1} n_j^{(1)}=0 \tag{11}$$

In addition, it will be assumed that the following conditions are satisfied:

$$\sigma_{zz}^{(1)} \xrightarrow[r\to\infty]{} p,\ \sigma_{ij}^{(1)} \xrightarrow[r\to\infty]{} p,\ (ij)\neq zz \tag{12}$$

Solution method

The problem, in which mathematical formulation is expressed in the previous subsection, is a boundary-value problem given for the system of non-linear PDE. In the investigation of this problem, the perturbation method, that is detailed in [2] and [3], will be applied. The quantities sought according to this method are expressed as the series of the small ε parameter, given in eq. (13), which is located in the equation of the middle line of the CNT given in eq. (1) and shows its degree of bending:

$$\sigma_{rr}^{(k)}=\sum_{q=0}^{\infty}\varepsilon^q\sigma_{rr}^{(k),q},...,\varepsilon_{rr}^{(k)}=\sum_{q=0}^{\infty}\varepsilon^q\varepsilon_{rr}^{(k),q},...,u_r^{(k)}=\sum_{q=0}^{\infty}\varepsilon^q u_r^{(k),q} \tag{13}$$

In addition, the eq. (2) and the expressions (3) of the unit normal vector of this surface can be obtained as a series of parameter ε:

$$\begin{gathered} r=R+\sum_{k=1}^{\infty}\varepsilon^k a_{rk}(\theta,t_3),\ z=t_3+\sum_{k=1}^{\infty}\varepsilon^k a_{zk}(\theta,t_3) \\ n_r=1+\sum_{k=1}^{\infty}\varepsilon^k b_{rk}(\theta,t_3),\ n_\theta=\sum_{k=1}^{\infty}\varepsilon^{\mathrm{k}} b_{\theta k}(\theta,t_3),\ n_z=\sum_{k=1}^{\infty}\varepsilon^k b_{zk}(\theta,t_3) \end{gathered} \tag{14}$$

For the 0th approximation, the eqs. (5)-(7) will be satisfied exactly. The eqs. (8)-(11) contact conditions will be satisfied exactly in $r=R-h^{(1)}$, $r=R-h^{(1)}-d$, $r=R-h^{(1)}-h^{(2)}-d$, $r=R-h^{(1)}-h^{(2)}-2d$, and $r=R-h^{(1)}-h^{(2)}-h^{(3)}-2d$ considering that $n_r=1$, $n_\theta=0$, and $n_z=0$. Apart from that, expressions (12) are written as follows for the zeroth approximation:

$$\sigma_{zz}^{(1),0} \xrightarrow[r\to\infty]{} p,\ \sigma_{zz}^{(1),0} \xrightarrow[r\to\infty]{} 0,\ \ (ij)\neq zz \tag{15}$$

In this way, the contact conditions and equations obtained for the 0th approximation are non-linear. The 0th approximation is the boundary value problem that needs to be investigated in order to determine the stress and strain that occurs when the CNT in the originally expressed model does not have local curvature, that is, it is flat. The relevant scientific views state that non-linear terms in the equations obtained for the 0th approximation in such a case will not have a significant effect and can be neglected [3]. For the validity of this assumption, assuming that $\nabla_n u^{(k)j,0}\ll 1$ condition is satisfied, the terms $g_p^j+\nabla_p u^{(1)j,0}$ will be replaced by δ_n^j which are Kronecker symbols. Thus, to achieve the 0th approximation:

$$\begin{gathered} \nabla_i\sigma^{(l)ij,0}=0,\ 2\varepsilon_{jq}^{(l),0}=\nabla_j u_i^{(l),0}+\nabla_q u_j^{(l),0} \\ \sigma_{(ij)}^{(l)}=\left(\lambda^{(l)}e^{(l),0}\right)\delta_i^n+2\left(\mu^{(l)}\varepsilon_{(ij)}^{(l),0}\right),\ e^{(l),0}=\mu^{(l)}\varepsilon_{(ii)}^{(l),0},\ i=r,\theta,z \end{gathered} \tag{16}$$

$$\sigma_{(ij)}^{(4),0}\Big|_{r=R-h^{(1)}-h^{(2)}-h^{(3)}-2d}=0,\ \sigma_{(ij)}^{(4),0}\Big|_{r=R-h^{(1)}-h^{(2)}-2d}=\sigma_{(ij)}^{(3),0}\Big|_{r=R-h^{(1)}-h^{(2)}-2d}$$
$$\sigma_{(ij)}^{(3),0}\Big|_{r=R-h^{(1)}-h^{(2)}-d}=\sigma_{(ij)}^{(4),0}\Big|_{r=R-h^{(1)}-h^{(2)}-d},\ \sigma_{(ij)}^{(2),0}\Big|_{r=R-h^{(1)}-d}=\sigma_{(ij)}^{(3),0}\Big|_{r=R-h^{(1)}-d}$$
$$\sigma_{(ij)}^{(2),0}\Big|_{r=R-h^{(1)}}=\sigma_{(ij)}^{(3),0}\Big|_{r=R-h^{(1)}},\ \sigma_{(ij)}^{(2),0}\Big|_{r=R}=\sigma_{(ij)}^{(1),0}\Big|_{r=R} \tag{17}$$
$$u_i^{(2),0}\Big|_{r=R}=u_i^{(1),0}\Big|_{r=R},\ (ij)=rr,r\theta,rz,\ (i)=r,\theta,z$$

are obtained. In the solution of eqs. (16) and (17), boundary conditions are given in eq. (15) must also be taken into consideration. Thus, the mathematical formulation of the problem that needs to be solved in order to achieve the 0th approximation is obtained.

Solution of the boundary value problem

At this stage, solutions of boundary value problems of 0th and first approximations, whose mathematical formulation was given in the previous sections, will be examined. The Poisson ratios of matrix material, outer, middle and inner CNT materials, respectively, are ν_1, ν_2, ν_3, and ν_4. For simplicity, it will be assumed that $\nu^{(1)}=\nu^{(2)}=\nu^{(3)}=\nu^{(4)}$. Taking Poisson ratios equal does not have a significant effect on numerical results according to [3]. Therefore, the $\nu^{(1)}=\nu^{(2)}=\nu^{(3)}=\nu^{(4)}$ condition will only be assumed in order to facilitate operations. In this case, the solution of the problem (15)-(17) can be obtained as follows for the 0th approximation:

$$\varepsilon_{zz}^{(1),0}=\varepsilon_{zz}^{(2),0}=\varepsilon_{zz}^{(3),0}=\varepsilon_{zz}^{(4),0}=\frac{p}{E^{(1)}}$$
$$u_z^{(1),0}=u_z^{(2),0}=u_z^{(3),0}=u_z^{(4),0}=\frac{p}{E^{(1)}}z,\ u_r^{(4),0}=-\nu^{(4)}\varepsilon_{zz}^{(4),0}r$$
$$u_r^{(2),0}=-\nu^{(2)}\varepsilon_{zz}^{(2),0}r,\ u_r^{(1),0}=-\nu^{(1)}\varepsilon_{zz}^{(1),0}r,\ u_\theta^{(1),0}=u_\theta^{(2),0}=u_\theta^{(3),0}=u_\theta^{(4),0}=0,\ \sigma_{zz}^{(1),0}=p$$
$$\sigma_{rr}^{(1),0}=\sigma_{rr}^{(2),0}=\sigma_{rr}^{(3),0}=\sigma_{rr}^{(4),0}=\sigma_{\theta\theta}^{(1),0}=\sigma_{\theta\theta}^{(2),0}=\sigma_{\theta\theta}^{(3),0}=\sigma_{\theta\theta}^{(4),0}=0$$
$$\sigma_{zz}^{(4),0}=p\frac{E^{(4)}}{E^{(1)}},\ \sigma_{zz}^{(3),0}=p\frac{E^{(3)}}{E^{(1)}} \tag{18}$$
$$\sigma_{zz}^{(2),0}=p\frac{E^{(2)}}{E^{(1)}},\ \sigma_{\theta z}^{(1),0}=\sigma_{\theta z}^{(2),0}=\sigma_{\theta z}^{(3),0}=\sigma_{\theta z}^{(4),0}=\sigma_{rz}^{(1),0}=\sigma_{rz}^{(2),0}=$$
$$=\sigma_{rz}^{(3),0}=\sigma_{rz}^{(4),0}=\sigma_{r\theta}^{(1),0}=\sigma_{r\theta}^{(2),0}=\sigma_{r\theta}^{(3),0}=\sigma_{r\theta}^{(4),0}=0$$

Let us consider the solution of the problem related to the first approximation. Within the framework of the assumptions made previously and taking into account the eq. (18), the governing field equations in cylindrical co-ordinates can be obtained [8]. By providing directly, these governing field equations coincide with equations 3-D linearized theory of elasticity (TDLTE) [33]. The strain-displacement equations can be seen in [34]. Let the equation of the centerline of the CNT, which we express with eq. (1):

$$x_1=A\exp\left[-\left(\frac{x_3}{L}\right)^2\right]\cos\left(m\frac{x_3}{L}\right)=\varepsilon L\exp\left[-\left(\frac{x_3}{L}\right)^2\right]\cos\left(m\frac{x_3}{L}\right)=\varepsilon\delta(x_3),\ \varepsilon=\frac{A}{L} \tag{19}$$

Parameter ε in eq. (19) is selected as $\varepsilon = A/L$ under $L > A$ assumption. The contact conditions for the first approximation are taken into account:

$$\left[\sigma_{rr}^{(1),1}-\sigma_{rr}^{(2),1}\right]\Big|_{r=R}=0,\ \left[\sigma_{r\theta}^{(1),1}-\sigma_{r\theta}^{(2),1}\right]\Big|_{r=R}=0,\ \left[\sigma_{rz}^{(1),1}-\sigma_{rz}^{(2),1}\right]\Big|_{r=R}=\left[\sigma_{zz}^{(1),0}-\sigma_{zz}^{(2),0}\right]\frac{\mathrm{d}\delta(t_3)}{\mathrm{d}t_3}\cos\theta$$

$$\left(u_r^{(1),1}-u_r^{(2),1}\right)\Big|_{r=R}=0,\ \left(u_\theta^{(1),1}-u_\theta^{(2),1}\right)\Big|_{r=R}=0,\ \left(u_z^{(1),1}-u_z^{(2),1}\right)\Big|_{r=R}=0,\ \sigma_{r\theta}^{(2),1}\Big|_{r=R\text{-}h^{(1)}}=0$$

$$\left[R-h^{(1)}\right]\sigma_{rr}^{(2),1}\Big|_{r=R-h^{(1)}}=c\left[u_r^{(2)}\Big|_{r=R-h^{(1)}}-u_r^{(3)}\Big|_{r=R-h^{(1)}-d}\right],\ \sigma_{rz}^{(2),1}\Big|_{r=R-h^{(1)}}=\sigma_{zz}^{(2),0}\frac{\mathrm{d}\delta(t_3)}{\mathrm{d}t_3}\cos\theta$$

$$\left(R-h^{(1)}\right)\sigma_{rr}^{(2),1}\Big|_{r=R-h^{(1)}}=\left(R-h^{(1)}-d\right)\sigma_{rr}^{(3),1}\Big|_{r=R-h^{(1)}-d}$$

$$\sigma_{r\theta}^{(3),1}\Big|_{r=R-h^{(1)}-d}=0,\ \sigma_{rz}^{(3),1}\Big|_{r=R-h^{(1)}-d}=\sigma_{zz}^{(3),0}\frac{\mathrm{d}\delta(t_3)}{\mathrm{d}t_3}\cos\theta$$

$$\left[R-h^{(1)}-h^{(2)}-d\right]\sigma_{rr}^{(3),1}\Big|_{r=R-h^{(1)}-h^{(2)}-d}=c\left[u_r^{(3)}\Big|_{r=R-h^{(1)}-h^{(2)}-d}-u_r^{(4)}\Big|_{r=R-h^{(1)}-2d}\right] \tag{20}$$

$$\sigma_{r\theta}^{(3),1}\Big|_{r=R-h^{(1)}-h^{(2)}-d}=0,\ \sigma_{rz}^{(3),1}\Big|_{r=R-h^{(1)}-h^{(2)}-d}=\sigma_{zz}^{(3),0}\frac{\mathrm{d}\delta(t_3)}{\mathrm{d}t_3}\cos\theta$$

$$\left[R-h^{(1)}-h^{(2)}-d\right]\sigma_{rr}^{(3),1}\Big|_{r=R-h^{(1)}-h^{(2)}-d}=\left[R-h^{(1)}-h^{(2)}-2d\right]\sigma_{rr}^{(4),1}\Big|_{r=R-h^{(1)}-h^{(2)}-2d}$$

$$\sigma_{r\theta}^{(4),1}\Big|_{r=R-h^{(1)}-h^{(2)}-2d}=0$$

$$\sigma_{rz}^{(4),1}\Big|_{r=R-h^{(1)}-h^{(2)}-2d}=\sigma_{zz}^{(4),0}\frac{\mathrm{d}\delta(t_3)}{\mathrm{d}t_3}\cos\theta,\ \sigma_{rr}^{(4),1}\Big|_{r=R-h^{(1)}-h^{(2)}-h^{(3)}-2d}=0$$

$$\sigma_{r\theta}^{(4),1}\Big|_{r=R-h^{(1)}-h^{(2)}-h^{(3)}-2d}=0,\ \sigma_{rz}^{(4),1}\Big|_{r=R-h^{(1)}-h^{(2)}-h^{(3)}-2d}=\sigma_{zz}^{(4),0}\frac{\mathrm{d}\delta(t_3)}{\mathrm{d}t_3}\cos\theta$$

For the solution of these equations notation in [33] resource are used. To solve the first approximation of the aforementioned boundary value problem, all related equations the exponential Fourier transform given in [8] is applied according to $z = x_3/L$. After applying Fourier transformation all related equations, related differential equations are solved by taking into account the equilibrium equations and contact conditions:

$$\overline{\gamma}^{(1),1}=\overline{A}_1^{(1)}(s)K_1\left[\xi_1^{(1)}s\frac{r}{L}\right]\sin\theta,\ \overline{\beta}^{(1),1}=i\left\{\overline{A}_2^{(1)}(s)K_1\left[\xi_2^{(1)}s\frac{r}{L}\right]+\overline{A}_3^{(1)}(s)K_1\left[\xi_3^{(1)}s\frac{r}{L}\right]\right\}\cos\theta$$

$$\overline{\gamma}^{(k),1}=\left[\overline{B}_{11}^{(k)}(s)I_1\left(\xi_1^{(2)}s\frac{r}{L}\right)+\overline{B}_{12}^{(k)}(s)K_1\left(\xi_1^{(2)}s\frac{r}{L}\right)\right]\sin\theta,\ k=2,3,4 \tag{21}$$

$$\overline{\beta}^{(k),1}=$$

$$=i\left\{\overline{B}_{21}^{(k)}(s)I_1\left[\xi_2^{(2)}s\frac{r}{L}\right]+\overline{B}_{22}^{(k)}(s)K_1\left[\xi_2^{(2)}s\frac{r}{L}\right]+\overline{B}_{31}^{(k)}(s)I_1\left[\xi_3^{(2)}s\frac{r}{L}\right]+\overline{B}_{32}^{(k)}(s)K_1\left[\xi_3^{(2)}s\frac{r}{L}\right]\right\}\cos\theta$$

The aforementioned equations are obtained. Here $K_n(x)$ are Macdonald functions and $I_n(x)$ are Bessel functions. When the functions in eq. (21) are replaced in the related equations, a linear equation system of 21 × 21 is obtained. After solving this system, the unknowns:

$$\overline{A}_1^{(1)}(s),\ \overline{A}_2^{(1)}(s),\ \overline{A}_3^{(1)}(s),...,\ \overline{B}_{32}^{(4)}(s)$$

are determined. By using

$$\overline{\sigma}_{\tau\tau}^{(1),1},...,\ \overline{\sigma}_{zz}^{(2),1}$$

with Fourier transform applied are calculated. In order to reach the real values of the stresses obtained, inverse Fourier Transform is applied. Thus, the solution of the boundary value problem related to the first approximation is made.

Numerical results

Integral $\int_{-\infty}^{+\infty}(.)\mathrm{d}s$ in inverse transformation becomes $\int_{0}^{+\infty}(.)\mathrm{d}s$ because the quantities are even or odd. In the solution of this integral, the following approach is taken into consideration

$$\int_0^{+\infty}(.)\mathrm{d}s \cong \int_0^{S_*}(.)\mathrm{d}s \cong \sum_{j=0}^{M}\int_{S_j}^{S_{j+1}}(.)\mathrm{d}s$$

with convergence criterion, values of $S_0 = 0$ and $S_M = S_*$ parameters were determined and selected as M and S_*. Also, Gauss-Legendre 10 point rule numerical integration method was used for numerical calculation of $\int_{S_j}^{S_{j+1}}(.)\mathrm{d}s$ integrals. Researches on stress distribution have been done in the scope of obtaining and interpreting the numerical results that depend on various parameters related to normal stresses σ_{nn}, σ_{ee}, and $\sigma_{\tau\tau}$. These stresses are on the surface S_6 in which matrix and CNT intersect. They are the stresses in the direction of the **n** unit normal vector, the **τ**, **e** tangent vectors and the planes formed by these vectors.

For numerical results, we suppose that R is the outermost radius, $h^{(1)}$ is the thickness of the outer tube, $h^{(2)}$ is the thickness of the middle tube, $h^{(3)}$ is the thickness of the inner tube, d is the distance between adjacent surfaces of the inner and outer tube. In addition, we define the parameters $\kappa_1 = R/L$, $\kappa_2 = h^{(1)}/R$, $\kappa_3 = d/h^{(1)}$, $\kappa_4 = h^{(2)}/R = \kappa_2$, and $\kappa_5 = h^{(3)}/R = \kappa_2$. The thicknesses of the walls of the CNT were considered as equal, $h^{(1)} = h^{(2)} = h^{(3)}$. Considering that the material is CNT, the following ranges are determined for these parameters to be used in calculations [32]. However, the ranges used for the TWCNT have been purified $200 \le E^{(2)}/E^{(1)} \le 1000$, $0.015 \le h^{(1)}/R \le 0.4$, $1 \le d/h^{(1)} \le 2$. Radial displacements on adjacent surfaces of inner, middle and outer tubes resist Van der Waals forces. For these forces to occur, the distance between adjacent surfaces of CNT must be less than 0.34 nm ($d \le 0.34$ nm) [13]. For the constant c, which represents the Van der Waals forces, $0 < c \le 9.92$ TPa range was taken [32]. Furthermore, parameter F has been defined to characterize the effect of Van der Waals forces on parameters:

$$F = \frac{\mu_{\mathrm{CNT}}}{c}\left(1 - \frac{h^{(1)}}{R}\right)$$

Note that the value $F = 0$ corresponds to the situation where the Van der Waals force between the tubes of the TWCNT is equal to zero, and the displacements of the tubes in the radial direction are equal to each other. However, the value of $F = \infty$ corresponds to the situation where the radial forces (stresses) acting on said cylindrical surfaces of the tubes are equal to zero. As a result, $F = \infty$ means no contact between the tubes of the TWCNT [32] (the CNT symbol in the μ_{CNT} parameter represents the carbon nanotube and $\mu_{\mathrm{CNT}} = \mu^{(2)} = \mu^{(3)} = \mu^{(4)}$). In addition, $\nu^{(1)} = \nu^{(2)} = \nu^{(3)} = \nu^{(4)} = 0.3$, $\varepsilon = 0.7$, and $E^{(2)}/E^{(1)} = 500$ values are used unless stated otherwise. Parameter $\alpha = \mathrm{p}/E^{(1)}$ is used to express the effect of geometric non-linearity on stress distribution. In tables

and figures that show the change of stresses according to the parameters aforementioned, $\theta = 0$ for σ_{nn}, $\sigma_{\tau\tau}$, σ_{ee}, and $x_3/L = 0$ for σ_{nn}, $\sigma_{\tau\tau}$, σ_{ee}, were used. In tables and figures showing the change of stresses according to $\kappa_1 = R/L$ parameter, $\theta = 0$ was used for σ_{nn}, $\sigma_{\tau\tau}$, σ_{ee}. In tables and figures showing the change of stresses according to $\kappa_2 = h^{(1)}/R$ parameter, $\theta = 0$ was used for σ_{nn}, $\sigma_{\tau\tau}$, σ_{ee}.

Figure 2 shows the relationship between $\sigma_{nn}/|p|$, $\sigma_{\tau\tau}/|p|$, $\sigma_{ee}/|p|$, and $\kappa_1 = R/L$ parameters for $\kappa_2 = 0.125$, $\kappa_3 = 1.5$ values and the effect of geometric non-linearity, α, on it. From these graphs, it is seen that the absolute values of $\sigma_{nn}/|p|$, $\sigma_{\tau\tau}/|p|$, $\sigma_{ee}/|p|$ in compression (tension) increase (decrease) non-monotonously with $|\alpha|$.

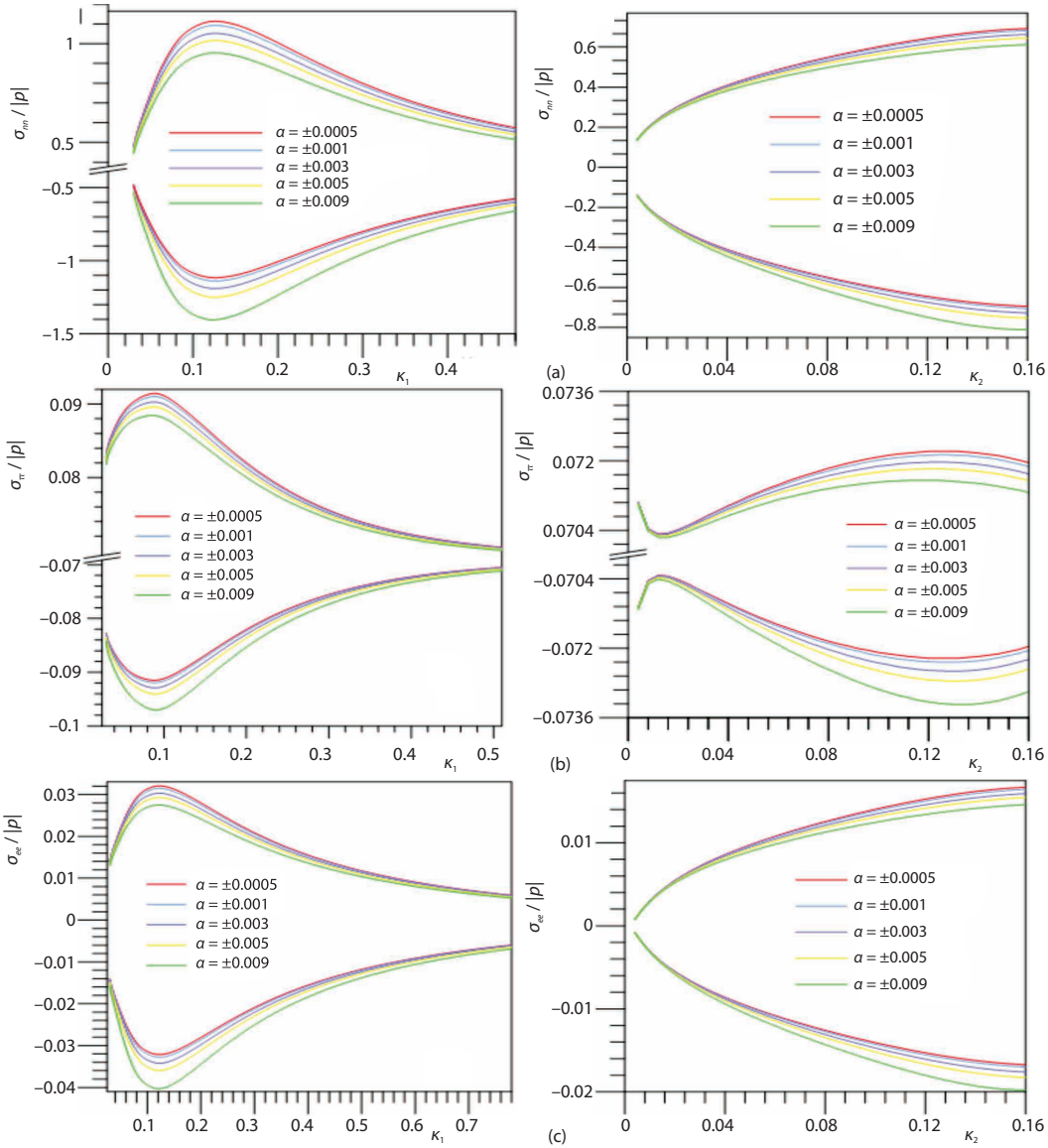

Figure 2. Dependencies between κ_1, κ_2 and (a) $\sigma_{nn}/|p|$, (b) $\sigma_{\tau\tau}/|p|$, (c) $\sigma_{ee}/|p|$ for various α ($E^{(2)}/E^{(1)} = 500$, $m = 0$, $\varepsilon = 0.07$, and $F = 100$)

In tab. 1, values of $\sigma_{nn}/|p|$ are given according to various m, α, $E^{(1)}/E^{(2)}$ parameters. Here, the numerical results of the stress values reached as a result of the 0th and first approach can be seen. From this table, it is observed that as the $E^{(2)}/E^{(1)}$ increase, the absolute value of $\sigma_{nn}/|p|$ increase. Apart from this, it is observed that as the $|\alpha|$ parameter increase, the absolute values of the stresses increase in compression and decrease in tension.

Table 1. Values of stress for various $E^{(2)}/E^{(1)}$, m and α ($\kappa_1 = 0.4$, $\kappa_2 = 0.125$, $\kappa_3 = 1.5$, $F = 100$)

	m	$E^{(2)}/E^{(m)}$	Tension					Compression				
			0.00005	0.001	0.003	0.005	0.009	–0.00005	–0.001	–0.003	–0.005	–0.009
$\sigma_{nn}/\|p\|$	0	300	0.52193	0.51592	0.50394	0.49276	0.47243	–0.52257	–0.52881	–0.54273	–0.55784	–0.59246
		500	0.65277	0.64376	0.62587	0.6093	0.57951	–0,65374	–0.66316	–0.68429	–0.70746	–0.76139
		1000	0.85343	0.83817	0.80824	0.78096	0.73295	–0.85508	–0.87118	–0.90786	–0.94891	–1.04812
	1	300	0.5676	0.56172	0.54994	0.53891	0.51875	–0.56823	–0.57433	–0.58791	–0.60258	–0.63599
		500	0.68528	0.67676	0.6598	0.64403	0.61554	–0.68619	–0.69508	–0.71497	–0.73668	–0.78693
		1000	0.85861	0.8448	0.81765	0.7928	0.74884	–0.8601	–0.87464	–0.90765	–0.94446	–1.03286
$\sigma_{\tau\tau}/\|p\|$	0	300	0.0706	0.07055	0.07046	0.07037	0.07022	–0.0706	–0.07065	–0,07076	–0.07088	–0.07117
		500	0.07222	0.07214	0.07197	0.07182	0.07155	–0.07223	–0.07232	–0.07252	–0.07275	–0.07328
		1000	0.0753	0.07512	0.07476	0.07444	0.07389	–0.07532	–0.07551	–0.07596	–0.07646	–0.07769
	1	300	0.06925	0.06921	0.06914	0.06907	0.06895	–0.06925	–0.06929	–0.06938	–0.06948	–0.06971
		500	0.07055	0.07049	0.07035	0.07023	0.07001	–0.07056	–0.07063	–0.0708	–0.07098	–0.07141
		1000	0.07303	0.07288	0.0726	0.07234	0.07189	–0.07305	–0.07321	–0.07357	–0.07398	–0.07498
$\sigma_{ee}/\|p\|$	0	300	0.01178	0.01164	0.01134	0.01106	0.01055	–0.0118	–0.01196	–0.0123	–0.01268	–0.01354
		500	0.01553	0.01529	0.01483	0.01439	0.01362	–0.01555	–0.0158	–0.01635	–0.01696	–0.01837
		1000	0.02137	0.02095	0.02013	0.01939	0.01809	–0.02141	–0.02185	–0.02286	–0.02398	–0.02671
	1	300	0.01134	0.0112	0.01092	0.01066	0.01019	–0.01135	–0.0115	–0.01182	–0.01217	–0.01297
		500	0.01463	0.01442	0.01399	0.0136	0.01289	–0.01465	–0.01488	–0.01538	–0.01593	–0.0172
		1000	0.01961	0.01924	0.01853	0.01787	0.01672	–0.01965	–0.02004	–0.02092	–0.0219	–0.02428

Conclusion

In this paper, stress analysis of composite material under evenly distributed normal forces was investigated depending on various parameters. Stress distribution on the TWCNT with locally curved is investigated for the first time in the literature with an approximately analytical method in 3-D. When the distance d, the gap between the tubes, is approached to zero as the limit, the result was same with the stress values obtained for the single-walled CNT. When the mechanical properties of CNT are examined in terms of elasticity constants, the E^{CNT}/E^{M} ratio appears to be much larger than the ratio for any composite material, where E^{CNT} and E^{M}, respectively are the elasticity constants for nanotube and matrix. In this study, these rates were taken as 300, 500, and 1000. Also, normal stresses were examined accordingly. It was seen that as the number of walls in nanotube was increased, the stress values reduced. The absolute values of $\sigma_{nn}/|p|$, $\sigma_{\tau\tau}/|p|$, $\sigma_{ee}/|p|$ in compression (tension) increase (decrease) with $|\alpha|$ parameter which express geometrically non-linearity. It is compatible with

the results available in the literature. As expected, the results obtained when $\alpha = \pm 5.10^{-5}$ seem to be the same with the results in the geometric linear state. Additionally, the values of $\sigma_{nn}/|p|$, $\sigma_{\tau\tau}/|p|$, $\sigma_{ee}/|p|$ have been obtained according to the change of R/L, $h^{(1)}/R$, and $d/h^{(1)}$ parameters, respectivly external radius of nanotube, the thickness of each nanotube and the spacing between the walls of the nanotube. In TWCNT, as the value of $E^{(2)}/E^{(1)}$ increases, the absolute values of $\sigma_{nn}/|p|$, $\sigma_{\tau\tau}/|p|$, $\sigma_{ee}/|p|$ are observed to increase. Considering all these results obtained during the course of the production of composite materials containing CNT, as well as considering the performance expected from the material, the radius length of the reinforcing material (here CNT) and the number of walls it should have can be estimated.

Acknowledgement

Funding: This study has been supported by Yıldız Technical University Scientific Research Projects Coordination Department. Project No. 2013-07-03-DOP01

References

[1] Akbarov, S. D., Guz, A. N., Stress State of a Fiber Composite with Curved Structures with a Low Fiber Concentration, *Soviet Applied Mechanics, 21* (1985), 6, pp. 560-565
[2] Akbarov, S. D., Guz, A. N., Method of Solving Problems in the Mechanics of Fiber Composites with Curved Structures, *Soviet Applied Mechanics*, *20* (1985c), 9, pp. 777-790
[3] Akbarov, S. D., Guz, A.nN., *Mechanics of Curved Composites*, Kluwer Academic Publishers, Amsterdam, The Netherlands, 2000
[4] Akbarov, S. D., Guz, A. N., Mechanics of Curved Composites (Piecewise Homogeneous Body Model), *International Applied Mechanics*, *38* (2002), 12, pp. 1415-1439
[5] Akbarov, S. D., Guz, A. N., Mechanics of Curved Composites and Some Related Problems for Structral Members, *Mechanics of Advanced Materials and Structures, 11* (2004), 6, pp. 445-515
[6] Akbarov, S. D., Kosker, R., On a Stresss Analysis in the Infinite Elastic Body with Two Neighbouring Curved Fibers, *Composites Part B*, *34* (2003), 2, pp. 143-150
[7] Akbarov, S. D., Kosker, R., Internal Stability Loss of Two Neighboring Fibers in a Viscoelastic Matrix, *Internal Journal of Engineering Science*, *42* (2004), 17-18, pp. 1847-1873
[8] Coban F., The Stress Distribution of an Infinite Body Containing a Single Locally Curved and Hollow Fiber, M. Sc. thesis (in Turkish), Yildiz Technical University, Istanbul, Turkey, 2009
[9] Hutchens, S. B., *et al*., Analysis of Uniaxial Compression of Vertically Aligned Carbon Nanotubes, *Journal of the Mechanics and Physics of Solids*, *59* (2011), 10, pp. 2227-2237
[10] Yeh, M. K., *et al*., Fabrication and Mechanical Properties of Multi-Walled Carbon Nanotubes/Epoxy Nanocomposites, *Materials Science and Engineering A*, pp. 483-484, (2006), June, pp. 289-292
[11] Yeh, M. K., *et al*., Mechanical Properties of Phenolic-Based Nanocomposites Reinforced by Multi-Walled Carbon Nanotubes and Carbon Fibers, *Composites Part A Applied Science and Manufacturing*, *39* (2008), 4, pp. 677-684
[12] Kalamkarov, A. L., *et al*., Analytical and Numerical Techniques to Predict Carbon Nanotubes Properties, *International Journal of Solids and structures*, *43* (2006), 22-23, pp. 6832-6854
[13] Xiaohu, Y., Qiang, H., Investigation of Axially Compressed Buckling of a Multi-Walled Carbon Nanotube Under Temperature Field, *Composite Science and Technology*, *67* (2006), 1, pp. 125-134
[14] Zhbanov, A., *et al*., Van der Waals Interaction Between Two Crossed Carbon Nanotubes, *ACS Nano*, *4* (2010), 10, pp. 5937-5945
[15] Li, C., Chou, T., A Structural Mechanics Approach for the Analysis of Carbon Nanotube, *International Journal of Solids and Structures*, *40* (2003), 10, pp. 2487-2499
[16] Ru, C. Q., Effect of van der Waals Forces on Axial Buckling of a Double-Walled Carbon Nanotubes, *Journal of Applied Physics*, *87* (2000), 10, pp. 7227-7231
[17] Shokrieh, M., Rafiee, R., Investigation of Nanotube Length Effect on the Reinforcement Efficiency in Carbon Nanotube Based Composites, *Composite Structures*, *92* (2010), 10, pp. 2415-2420
[18] Georgantzinos, S. K., *et al*., Investigation of Stress-Strain Behavior of Single Walled Carbon Nanotube/Rubber Composites by a Multi-Scale Finite Element Method, *Theoretical and Applied Fracture Mechanics*, *52* (2009), 3, pp. 158-164

[19] Ru, C. Q., Column Buckling of Multiwalled Carbon Nanotubes with Interlayer Radial Displacements, *Phys. Rev. B*., *62* (2000), 24, pp. 16962-16967
[20] Shen, H. S., Postbuckling Prediction of Double-Walled Carbon Nanotubes under Hydrostatic Pressure, *International Journal of Solids and Structures*, *41* (2004), 9, pp. 2643-2657
[21] Thai, H. T., A Non-Local Beam Theory for Bending, Buckling and Vibration of Nanobeams, *International Journal of Engineering Science*, *52* (2012), Mar., pp. 56-64
[22] Jochum, C. H., Grandidier, J. C., Microbuckling Elastic Modelling Approach of a Single Carbon Fibre Embedded in an Epoxy Matrix, *Composites Science and Technology*, *64* (2004), 16, pp. 2441-2449
[23] Lourie, O., *et al*., Buckling and Collapse of Embedded Carbon Nanotubes, *Physics Review Letters*, *81* (1998), 8, pp. 1638-1641
[24] Young, R. J., *et al*., The Mechanics of Graphene Nanocomposites a Review, *Composites Science and Technology*, *72* (2012), 12, pp. 1459-1476
[25] Guz, I. A., Continuum Solid Mechanics at Nanoscale How Small Can it Go, *Journal of Nanomaterials Molecules and Nanotechnology*, *1* (2012), 1, p. 1
[26] Duan, H. L., *et al*., Theory of Elasticity at the Nanoscale, *Advanced Applied Mechanics*, *42* (2009), 1, pp. 1-68
[27] Windle, A. H., Two Defining Moments A Personal View by Prof. Alan H. Windle, *Composites Science and Technology*, *67* (2007), 5, pp. 929-930
[28] Harik, V. M., Ranges of Applicability for the Continuum Beam Model in the Mechanics of Carbon Nanotubes and Nanorods, *Solid State Communications*, *120* (2001), 7-8, pp. 331-335
[29] Guz, A. N., Rushchidsky, J. J., Nanomaterials on the Mechanics of Nanomaterials, *International Applied Mechanics*, *39* (2003), 11, pp. 1271-1293
[30] Guz, A. N., Rushchidsky, J. J., *Short Introduction Mechanics of Nanocomposites*, Scientific & Academic Publishing, Rosemead, Cal., USA, 2012
[31] Coban, F., Stress and Stability Analysis of Double and Triple-Walled Carbon Nanotubes with Local Curvature, Ph. D. thesis (in Tutkish), Yıldız Technical University, Istanbul, Turkey, 2016
[32] Akbarov, S. D., Microbuckling of a Doublewalled Carbon Nanotube Embedded in an Elastic Matrix, *International of Solids and Structures*, *50* (2013), 16-17, pp. 2584-2596
[33] Guz, A. N., *Fundamentals of the 3-D Theory of Stability of Deformable Bodies*, Springer-Verlag, Berlin, 1999
[34] Kosker, R., On Internal Stability Loss of a Row Unidirected Periodically Located Fibers In the Visco-Elastic Matrix, *Thermal Science*, *23* (2019), S1, pp. S427-S438

Paper submitted: May 26, 2020
Paper revised: October 20, 2020
Paper accepted: October 28, 2020